Multiple excitation modes in ^{163}Hf

R. B. Yadav, W. C. Ma, J. C. Marsh, and Q. A. Ijaz
Department of Physics & Astronomy, Mississippi State University, Mississippi State, Mississippi 39762, USA

R. V. F. Janssens, M. P. Carpenter, C. R. Hoffman, T. Lauritsen, and S. Zhu
Physics Division, Argonne National Laboratory, Argonne, Illinois 60439, USA

F. G. Kondev and G. Gürdal
Nuclear Engineering Division, Argonne National Laboratory, Argonne, Illinois 60439, USA

G. B. Hagemann
The Niels Bohr Institute, Blegdamsvej 17, DK-2100 Copenhagen, Denmark

D. J. Hartley
Department of Physics, United States Naval Academy, Annapolis, Maryland 21402, USA

L. L. Riedinger
Department of Physics and Astronomy, University of Tennessee, Knoxville, Tennessee 37996, USA

S. Mukhopadhyay
Nuclear Physics Division, Bhabha Atomic Research Centre, Mumbai 400085, India

(Received 27 August 2014; revised manuscript received 28 October 2014; published 19 November 2014)

Excited states of ^{163}Hf were populated using the ^{94}Zr(^{74}Ge,5n) reaction and the decay γ rays were measured with the Gammasphere spectrometer. Two previously known bands were extended to higher spins, and nine new bands were identified. In addition to bands associated with three- and five-quasiparticle configurations, two γ-vibrational bands coupled to the $i_{13/2}$ excitation were also observed. The lowest level of a newly identified, negative-parity band is proposed to be the ground state of the nucleus. A systematic delay of the high-spin proton crossing frequency with increasing quadrupole deformation from ^{162}Hf to ^{172}Hf was established. Extensive band searches failed to reveal a triaxial, strongly deformed structure in ^{163}Hf similar to the one observed in several nuclei around $A \sim 165$.

DOI: 10.1103/PhysRevC.90.054325 PACS number(s): 21.10.Re, 23.20.Lv, 25.70.Gh, 27.70.+q

I. INTRODUCTION

High-spin collective motion associated with a stable triaxial nuclear shape has been investigated extensively in recent years for nuclei near $A \sim 165$. The wobbling mode, a characteristic motion of triaxial nuclei, has been established in the odd-Z, even-N nuclei $^{161-167}_{71}$Lu [1–5] and $^{167}_{73}$Ta [6]. In addition, triaxial strongly deformed (TSD) bands based on quasiparticle excitations, with deformation parameters $(\varepsilon_2,\gamma) \sim (0.4,20^\circ)$, have also been observed in the neighboring nuclei, such as in ^{162}Lu [7], ^{163}Lu [8], ^{164}Lu [9], $^{163}_{69}$Tm [10], and $^{168}_{72}$Hf [11,12]. Very recently, two TSD bands were identified in ^{164}Hf and linked to the known, normal deformed (ND), states [13]. This makes ^{164}Hf the first even-even system in the mass region where a detailed comparison of the observed and calculated properties of TSD bands could be performed. Based on the same data, a search for TSD bands in odd-A ^{163}Hf appeared worthwhile. Unfortunately, as discussed below, an exhaustive search yielded a negative result, even though a detailed study of normal deformed structures proved most fruitful. The latter forms the core of the present paper.

A previous spectroscopy study of ^{163}Hf by Blume *et al.* reports only two bands, built on the $\nu[651]3/2^+$ and $\nu[523]5/2^-$ orbitals [14]. Although the present study did not lead to the discovery of TSD bands in ^{163}Hf, several other noteworthy features were revealed. High-spin states up to $77/2^+$ were observed, and nine new bands were identified. A large number of interband linking transitions were established and, as a result, all the sequences have been linked. Proton crossings at $\hbar\omega \sim 0.45$ MeV were traced to their full alignments. Based on these results, and recent data in neighboring Hf isotopes, a systematic trend of a delayed proton crossing frequency with increasing quadrupole deformation from ^{162}Hf to ^{172}Hf could be established. A negative-parity band, built on the $\nu h_{9/2}$ shell-model state, was observed and its $5/2^-$ bandhead is proposed to be the ground state of the ^{163}Hf nucleus. Two positive-parity sequences are suggested to correspond to γ-vibrational bands built on the $i_{13/2}$ neutron excitation. The intrinsic configurations of all the bands are discussed within the framework of the cranked shell model, aided by comparisons with neighboring nuclei.

The experiment and the off-line data analysis are outlined in Sec. II, followed by a presentation of the main results in Sec. III. Section IV contains a more detailed discussion of the configuration assignments as well as of the nature of observed band crossings.

II. EXPERIMENTAL DETAILS AND RESULTS

High-spin states in ^{163}Hf were populated through the ^{94}Zr(^{74}Ge,5n) reaction, where the ^{74}Ge beam was accelerated to 330 MeV by the ATLAS facility at Argonne National Laboratory. The target consisted of a self-supporting thin foil ($\sim$0.76 mg/cm^2) of isotopically enriched ^{94}Zr. Coincident γ rays were measured using the Gammasphere array [15] which consisted of 99 Compton-suppressed Ge detectors at the time of the experiment. A total of 3.3×10^9 fourfold, or higher, prompt coincidence events were collected. The population ratio between the ^{164}Hf and ^{163}Hf reaction channels was about 2:1.

In the off-line analysis, the data were sorted into a database where the γ-ray energies and detector identification were stored for each event. The RADWARE software package [16] was used to construct three-dimensional (cube) and four-dimensional (hypercube) histograms, and to, subsequently, analyze the γ-ray coincidence relationships. The RADWARE band search routine was used extensively to look for weak high-spin bands. In addition, an analysis of γ-ray directional correlation from oriented states (DCO ratios) [17] was performed in order to determine the multipolarity of the γ rays. A number of gated DCO matrices were constructed from the database for this purpose. The extracted DCO ratios from $E2$-gated coincidence spectra fall into two distinct groups centered around 1.0 and 0.6 for stretched quadrupole and dipole transitions, respectively. Further discussion of the technique, including different gating conditions and DCO ratios of unstretched transitions, can be found in the previous publication of Ref. [18]. The parity assignments are based on the multipolarities of linking transitions between bands, as well as on coincidence relationships that introduce important constraints in some instances.

III. LEVEL SCHEME

The new level scheme from the present study is given in Fig. 1. The γ-ray decay sequences are numbered according to the order of the discussion below. They are also labeled by their low-spin quasiparticle configurations. For convenience of discussion, these sequences will be loosely referred to as "bands," as is customary, even though each sequence corresponds only to a signature of a band. Bands 1 and 4 were observed previously [14]; all others were identified here for the first time. Table I lists the energy levels and γ-ray transitions, as well as the measured γ-ray intensities and DCO ratios.

A. Bands 1–6

Bands 1 and 4 were identified previously [14]. Based on the level systematics and Nilsson model calculations, Blume *et al.* identified band 1 as the neutron $i_{13/2}$ sequence built on the $13/2^+$ state, and concluded that this state is not the ground state. The assigned positive parity for band 1 and negative

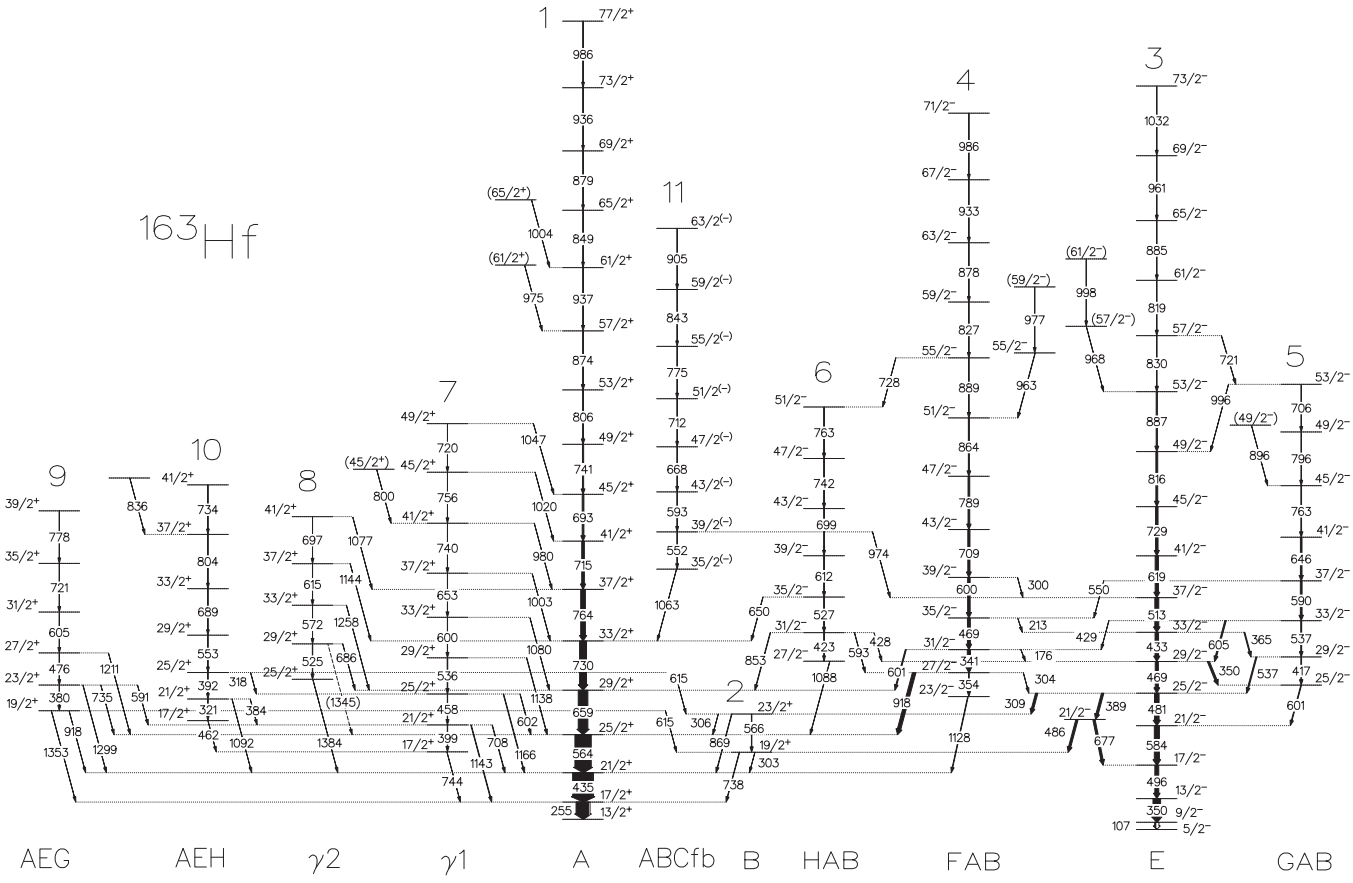

FIG. 1. Proposed level scheme for ^{163}Hf; energies are in keV and arrow widths are proportional to the relative intensities of the γ rays.

TABLE I. Spin and parity assignments for states in ^{163}Hf, as well as γ-ray energies, intensities, and DCO ratios. The level energies are given relative to the $5/2^-$ state in band 3. The intensities are normalized to the 435-keV ($21/2^+ \rightarrow 17/2^+$) transition in band 1, which has been assigned an intensity of 100.

J_i^π	E_i (keV)	E_γ (keV)[a]	I_γ	R_{DCO}[b]
		Band 1		
$13/2^+$	150.9			
$17/2^+$	406.3	255.4	61(2)	0.91(9)
$21/2^+$	840.8	434.5	100(3)	0.93(10)
$25/2^+$	1404.6	563.7	79(3)	0.96(11)
$29/2^+$	2063.2	658.6	47(2)	0.96(12)
$33/2^+$	2792.9	729.7	34(2)	0.99(13)
$37/2^+$	3556.4	763.5	23(2)	1.07(15)
$41/2^+$	4271.1	714.7	13(2)	0.94(14)
$45/2^+$	4964.2	693.1	8.3(9)	0.92(13)
$49/2^+$	5705.0	740.8	5.8(7)	0.92(13)
$53/2^+$	6510.9	805.9	4.1(5)	1.11(19)
$57/2^+$	7385.0	874.1	3.4(5)	1.14(18)
$61/2^+$	8322.2	937.2	1.74(28)	1.06(15)
$(61/2^+)$[c]	8360.0	975.0	<0.5	
$65/2^+$	9171.5	849.3	0.5(1)	
$(65/2^+)$[c]	9326.0	1003.8	<0.5	
$69/2^+$	10050.7	879.2	<0.5	
$73/2^+$	10986.4	935.7	<0.5	
$77/2^+$	11972.4	986.0	<0.5	
		Band 2		
$19/2^+$	1144.1	303.3	2.1(3)	1.03(16)[d]
		737.8	9(1)	1.3(2)
$23/2^+$	1710.3	305.7	0.57(9)	0.95(28)[d]
		566.2	3.1(5)	
		869.4	4.3(9)	1.3(2)
		Band 3		
$5/2^-$	0.0			
$9/2^-$	107.1	107.1	5.6(9)	0.95(13)
$13/2^-$	457.4	350.3	48(5)	0.97(12)
$17/2^-$	953.5	496.1	37(4)	0.90(14)
$21/2^-$	1537.8	584.3	24(3)	1.02(13)
$21/2^-$[c]	1630.0	676.5	11(2)	1.07(16)
		485.9	16(2)	0.63(8)
$25/2^-$	2019.0	481.2	19(2)	1.05(14)
		308.7	11(1)	0.56(6)
		389.0	12(2)	0.91(14)
$29/2^-$	2488.1	469.1	15(2)	1.02(14)
		349.5	4.5(7)	
$33/2^-$	2920.6	432.5	11(2)	1.13(14)
		364.7	3.3(5)	0.96(14)
$37/2^-$	3433.9	513.3	10(1)	0.95(10)
$41/2^-$	4053.2	619.3	8.7(9)	0.98(11)
$45/2^-$	4781.7	728.5	6.5(9)	0.95(12)
$49/2^-$	5597.4	815.7	4.7(8)	1.05(12)
$53/2^-$	6484.6	887.2	3.2(5)	0.94(13)
$57/2^-$	7314.4	829.8	1.3(2)	0.97(12)
		720.8	0.5(1)	0.94(17)
$(57/2^-)$[c]	7452.6	968.0	<0.5	
$61/2^-$	8133.6	819.2	0.84(16)	
$(61/2^-)$[c]	8450.6	998.0	1.2(2)	1.05(16)
$65/2^-$	9018.4	884.8	0.5(1)	1.07(17)
$69/2^-$	9979.6	961.2	<0.5	1.09(18)
$73/2^-$	11011.5	1031.9	<0.5	

TABLE I. (*Continued.*)

J_i^π	E_i (keV)	E_γ (keV)[a]	I_γ	R_{DCO}[b]
		Band 4		
$23/2^-$	1968.7	1127.9	2.8(4)	0.61(9)
$27/2^-$	2322.9	354.2	3.1(5)	0.98(13)
		303.9	0.53(9)	0.63(13)
		918.3	17(2)	0.65(11)
$31/2^-$	2664.1	341.3	15(2)	0.94(14)
		176.0	<0.5	
		600.9	4.8(8)	
$35/2^-$	3133.3	469.1	14(2)	0.94(12)
		212.6	<0.5	
$39/2^-$	3733.6	600.4	12.2(9)	0.89(16)
		299.7	<0.5	
$43/2^-$	4442.7	709.1	10.5(9)	0.92(13)
$47/2^-$	5231.6	788.9	8.3(8)	0.92(13)
$51/2^-$	6096.0	864.4	5.1(8)	1.07(12)
$55/2^-$	6985.3	889.3	2.0(3)	1.02(15)
		727.5	0.54(9)	
$55/2^-$[c]	7058.8	962.8	1.4(2)	1.09(16)
$59/2^-$	7812.3	827.0	1.2(2)	1.09(15)
$(59/2^-)$[c]	8036.1	977.3	0.63(2)	
$63/2^-$	8690.3	878.0	0.76(13)	0.94(14)
$67/2^-$	9623.1	932.8	0.5(1)	1.08(16)
$71/2^-$	10609.3	986.2	<0.5	
		Band 5		
$25/2^-$	2138.6	600.8	9(1)	1.06(15)
$29/2^-$	2555.9	417.3	2.6(6)	1.11(19)
		536.9	5.2(8)	0.98(10)
$33/2^-$	3092.8	536.9	8.6(9)	1.08(14)
		428.7	<0.5	
		604.7	2.7(4)	1.04(17)
$37/2^-$	3683.0	590.2	5.0(8)	1.04(15)
		549.8	1.4(2)	0.55(9)
$41/2^-$	4329.2	646.2	2.9(4)	1.08(11)
$45/2^-$	5092.6	763.4	3.3(6)	1.04(16)
$49/2^-$	5888.1	795.5	0.95(15)	0.95(13)
$(49/2^-)$[c]	5989.0	896.4	<0.5	
$53/2^-$	6593.6	705.5	0.5(1)	0.92(13)
		996.2	0.7(1)	
		Band 6		
$27/2^-$	2492.5	1087.9	0.84(16)	
$31/2^-$	2915.7	423.2	0.57(12)	
		427.6	<0.5	
		592.8	1.4(2)	0.97(13)
		852.5	2.3(4)	0.56(11)
$35/2^-$	3442.9	527.2	2.8(5)	1.14(18)
		650.0	1.4(2)	
$39/2^-$	4054.8	611.9	1.8(3)	0.97(13)
$43/2^-$	4753.4	698.6	0.67(13)	1.12(18)
$47/2^-$	5495.2	741.8	1.9(3)	0.90(17)
$51/2^-$	6257.8	762.6	2.3(4)	0.89(17)
		Band 7		
$17/2^+$	1150.2	743.9	0.9(2)	
$21/2^+$	1549.0	398.8	1.8(3)	0.90(13)
		708.2	2.0(3)	
		1142.7	2.7(3)	
$25/2^+$	2007.0	458.0	1.5(2)	1.06(16)
		602.4	0.93(15)	
		1166.2	2.6(4)	1.05(12)

TABLE I. (*Continued.*)

J_i^π	E_i (keV)	E_γ (keV)[a]	I_γ	R_{DCO}[b]
$29/2^+$	2542.8	535.8	2.7(3)	1.08(16)
		1138.2	1.6(3)	1.04(15)
$33/2^+$	3142.9	600.1	0.85(15)	1.16(18)
		1079.7	<0.5	
$37/2^+$	3795.9	653.0	0.62(9)	
		1003.0	<0.5	
$41/2^+$	4536.0	740.1	0.5(1)	
		979.6	0.5(1)	
$45/2^+$	5291.5	755.5	<0.5	
		1020.4	0.74(12)	
$(45/2^+)$[c]	5335.6	799.6	<0.5	
$49/2^+$	6011.1	719.6	<0.5	
		1046.9	<0.5	
		Band 8		
$25/2^+$	2224.8	1384.0	0.9(2)	
$29/2^+$	2749.3	524.5	1.9(3)	
		686.1	0.8(2)	
		(1344.7)	<0.5	
$33/2^+$	3321.4	572.1	1.5(3)	0.98(15)
		1258.2	1.1(2)	1.02(17)
$37/2^+$	3936.8	615.4	3.3(5)	0.96(13)
		1143.9	2.1(3)	0.94(15)
$41/2^+$	4633.6	696.8	2.5(4)	0.97(14)
		1077.2	1.5(3)	
		Band 9		
$19/2^+$	1759.1	615.0	0.72(13)	
		918.3	1.05(19)	
		1352.8	0.83(15)	
$23/2^+$	2139.5	380.4	0.89(15)	0.93(14)
		590.5	0.89(15)	0.64(10)
		734.9	0.54(8)	
		1298.7	1.2(2)	0.77(12)
$27/2^+$	2615.4	475.9	2.9(4)	1.07(17)
		1210.8	<0.5	
$31/2^+$	3220.8	605.4	1.8(3)	0.91(14)
$35/2^+$	3941.4	720.6	0.9(2)	1.09(15)
$39/2^+$	4719.7	778.3	<0.5	1.06(16)
		Band 10		
$17/2^+$	1612.6	462.4	<0.5	0.93(19)
$21/2^+$	1933.1	320.5	0.5(1)	
		384.1	0.6(1)	0.98(20)
		1092.3	<0.5	
$25/2^+$	2325.2	392.1	2.5(4)	0.92(15)
		318.2	0.5(1)	0.97(29)
		614.9	0.8(2)	
$29/2^+$	2878.2	553.0	2.4(4)	0.97(9)
$33/2^+$	3566.8	688.6	1.8(3)	0.94(14)
$37/2^+$	4370.4	803.6	0.9(2)	
$41/2^+$	5104.4	734.0	<0.5	
	5206.5[c]	836.1	<0.5	
		Band 11		
$35/2^{(-)}$	3856.3	1063.4	0.66(9)	0.63(18)
$39/2^{(-)}$	4407.9	551.6	0.6(1)	1.1(2)
		974.0	<0.5	
$43/2^{(-)}$	5000.4	592.5	0.5(1)	1.03(15)
$47/2^{(-)}$	5668.2	667.8	<0.5	1.02(12)
$51/2^{(-)}$	6380.4	712.2	<0.5	

TABLE I. (*Continued.*)

J_i^π	E_i (keV)	E_γ (keV)[a]	I_γ	R_{DCO}[b]
$55/2^{(-)}$	7155.6	775.2	<0.5	0.98(16)
$59/2^{(-)}$	7998.3	842.7	<0.5	0.90(14)
$63/2^{(-)}$	8903.1	904.8	<0.5	

[a]The uncertainties in the quoted γ-ray energies are 0.2 keV for most transitions, and 0.5 keV for weak ($I_\gamma < 1$) ones.
[b]DCO ratios were measured by gating on stretched-$E2$ transitions, unless indicated otherwise.
[c]Side-feeding levels associated with the bands.
[d]DCO ratios were measured by gating on stretched-dipole transitions.

parity for band 4 came from the proposed configurations of the bands, and the measured γ-ray angular correlation ratios. In the current study, band 1 is observed to be the most strongly populated sequence in ^{163}Hf. The measured DCO ratios for the transitions in bands 1 and 4, as well as those for the 918- and 1128-keV linking transitions between the two sequences, agree with previous spin assignments. Band 1 has now been extended from $57/2^+$ to $77/2^+$. The previously observed 963-keV γ ray at the highest spin $(55/2^-)$ of band 4 is now suggested to be associated with a side feeding to the $51/2^-$ level. Five new $E2$ transitions have been placed above this $51/2^-$ level as high-spin members, and band 4 has been extended to $71/2^-$, as a result.

Band 2 consists of only two states. The depopulating γ rays from the lower level feed the $21/2^+$ and $17/2^+$ states, and those from the upper one feed the $25/2^+$ and $21/2^+$ levels in band 1, respectively. The DCO ratios of the 303- and 306-keV γ rays are consistent with a stretched-dipole character. The DCO ratios of both the 738- and 869-keV γ rays indicate that they likely correspond to $M1/E2$ mixed transitions. Thus, the most likely scenario is that the two levels in band 2 have $23/2^+$ and $19/2^+$ respective quantum numbers and that both are depopulated via two $\Delta I = 1$ transitions.

Band 3 is a cascade of 17 transitions, 15 of which were determined to be stretched $E2$ in nature from their DCO ratios (see Table I). Bands 3 and 4 are connected by four linking transitions of 304, 176, 213, and 300 keV. The DCO ratio of the 304-keV transition, 0.63(13), is consistent with a stretched-dipole character, suggesting a link from the $27/2$ level in band 4 to the $25/2$ state in band 3. Further support comes from the 309-keV transition from this $25/2$ level to the $23/2^+$ state in band 2: its DCO ratio of 0.56(6) is consistent with a stretched-dipole nature. In addition, a branch of 389- and 486-keV γ rays depopulates this $25/2$ level in band 3 and feeds the $19/2^+$ state in band 2. The DCO ratios of the two transitions are consistent with stretched-$E2$ and dipole characters, respectively, suggesting that the former decays from $25/2$ to $21/2$, and the latter from $21/2$ to $19/2$. Based on such spin assignments, together with other rotational properties, including the excitation energies, aligned angular momenta, and moments of inertia, some of which will be discussed in detail in Sec. IV, bands 3 and 4 can be identified as signature partners. This requires band 3 to be of negative parity. This band has been identified from the $73/2^-$ state

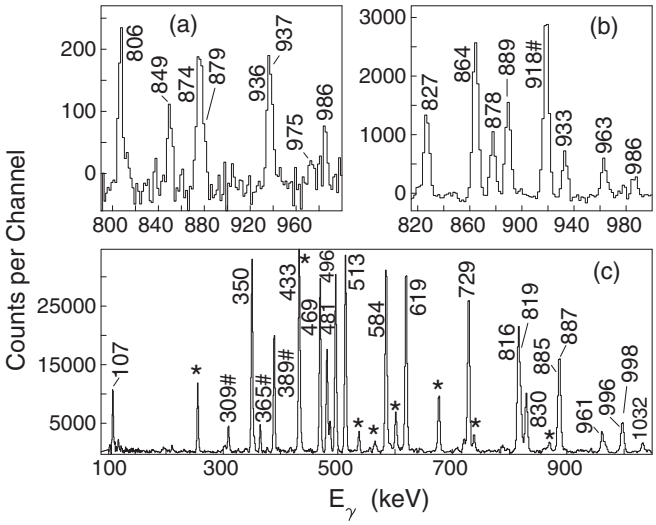

FIG. 2. Panels (a) and (b) display the high-spin extensions of bands 1 and 4, respectively, while (c) is a representative spectrum of band 3. The spectra of all the panels in this figure result from summing spectra where γ rays are in coincidence with three in-band transitions. For band 1, gates were set on transitions between the $41/2$ and $73/2$ levels, while for bands 3 and 4 gates were placed on all band members. The in-band transitions are labeled by energies. The following sign convention is used for the spectra in all figures: the stars ("$*$") denote coincident γ rays in other known bands, the pound signs ("#") mark the interband linking transitions, and the plus symbols ("+") indicate identified contaminations from other sources.

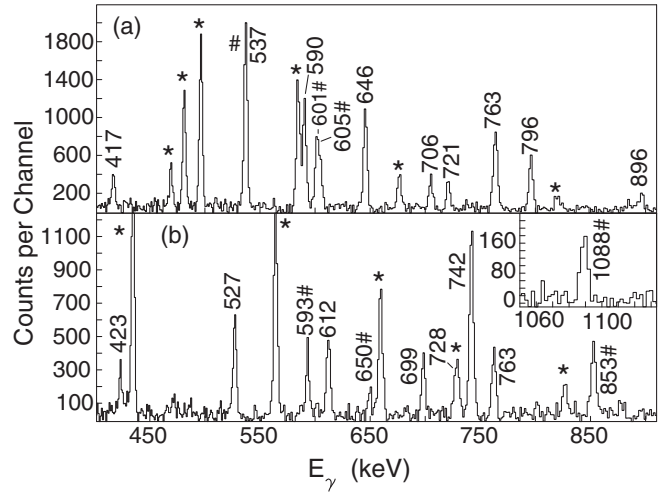

FIG. 3. Spectra of bands 5 (a) and 6 (b) produced by summing triple gates. For band 5, gates were set on any two band members and one of the four lowest transitions in band 3, while for band 6 gates were placed on any two band members (except for the 742-keV γ ray) and one of the three lowest transitions in band 1. The inset in panel (b) is a continuation of the main spectrum. The reader is referred to the caption of Fig. 2 for the definition of the symbols.

down to the $5/2^-$ level, which is the lowest state in the scheme of Fig. 1. Coincidence spectra representative of bands 1, 3, and 4 are displayed in Fig. 2.

Band 5 consists of a sequence of seven $E2$ transitions. Strong mixing is observed between bands 3 and 5 at lower spins with several stretched-$E2$ transitions (601, 537, and 605 keV) decaying from band 5 to band 3, and vice versa. Similar interband connections are also seen at the top of band 5. Thus, this sequence must have the same, negative parity as band 3, and its level quantum numbers can be determined. Further support comes from the 550-keV γ ray, decaying from the $37/2^-$ level in band 5 to the $35/2^-$ state in band 4. Its DCO ratio of 0.55(9) is consistent with a stretched-dipole, presumably $M1$, character.

Band 6 consists of six members and decays mainly to band 1 with 650-, 853-, and 1088-keV γ rays. The band is also linked to band 4 via a 593-keV transition at low spin, and a 728-keV one at high spin. The DCO ratio of the 593-keV γ ray, 0.97(13), is consistent with a stretched-$E2$ character, suggesting a decay from $31/2^-$ in band 6 to $27/2^-$ in band 4. Thus, band 6 has negative parity. This is further supported by the measured DCO ratio of the 853-keV decay-out γ ray, which is consistent with a stretched-dipole, presumably $E1$, character. The band is also linked with band 3 ($31/2^- \rightarrow 29/2^-$) through a 428-keV transition. Fourfold coincidence spectra for bands 5 and 6 are presented in Fig. 3.

B. Bands 7–11

A striking feature of bands 7 and 8 is that every level has a transition decaying directly into band 1. Such a behavior indicates that these two sequences are closely associated with the positive-parity, $i_{13/2}$ structure. The DCO ratio values of the 1166- and 1138-keV depopulating transitions from band 7, and those of the 1258- and 1144-keV γ rays from band 8 are 1.05(12), 1.04(15), 1.02(17), and 0.94(15), respectively; i.e., consistent with a stretched-$E2$ character. Therefore, bands 7 and 8 have been assigned positive parity and their level spins have been determined. The spectra of the two bands are displayed in Fig. 4.

Band 9 consists of five members. Its decay pathways fragment, feeding bands 1, 2, and 7, which are all of positive parity. This could be an indication that band 9 may be of the same parity. The DCO ratios of two decay-out transitions were measured. The 591-keV γ ray, feeding the $21/2^+$ level in band 7, has a DCO ratio of 0.64(10). The value suggests that the γ ray is likely of a stretched-dipole ($M1$ or $E1$) character, leading to a spin assignment of $23/2$ for the depopulating level. Furthermore, the 1299-keV transition linking this $23/2$ level and the $21/2^+$ state in band 1 has a DCO ratio of 0.77(12), which is between the expected values for a stretched-dipole and a stretched-quadrupole transition, but is consistent with a mixed $M1/E2$ γ ray. Consequently, band 9 has been assigned positive parity. A representative spectrum for band 9 is displayed in Fig. 5. A weak 832-keV γ ray depopulates the band, but cannot be firmly placed in the level scheme.

Band 10 has six members. Five of its depopulating transitions have been successfully identified to feed the positive-parity bands 1, 2, and 7, a behavior identical to that of band 9. Three depopulating transitions of 462, 384, and 318 keV, feed band 7; a 1092-keV γ ray feeds band 1, and a 615-keV line

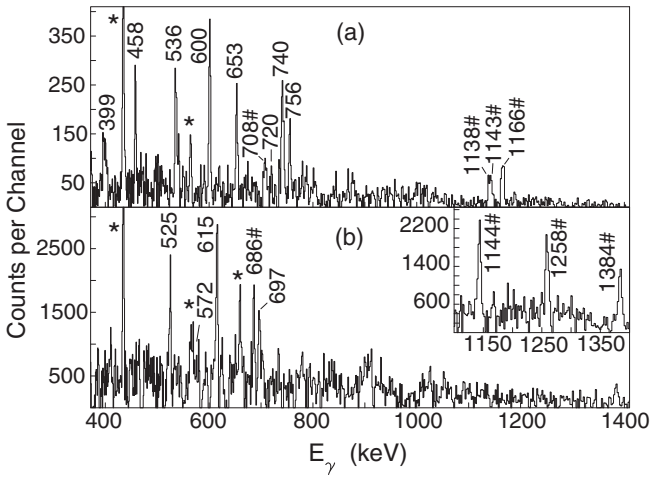

FIG. 4. (a) Fourfold coincidence spectrum of band 7, resulting from a sum of triple gates on all band members, and (b) triple coincidence spectrum of band 8. For the main spectrum, double gates were set on the 572-keV in-band transition and one of the four lowest transitions in band 1. For the inset, double gates were set on any band member and one of the two lowest transitions in band 1. The reader is referred to the caption of Fig. 2 for the definition of the symbols.

links to band 2. The DCO ratios of the 462-, 384- and 318-keV γ rays are all close to 1.0 (see Table I), indicating that these are either $\triangle I = 0$ dipole, or stretched-$E2$ transitions. The latter possibility can be ruled out, since this would make the excitation energy of the band nearly as low as that of the yrast band 1, which is in contrast with its weak population. In addition, this hypothesis would require the 615-keV interband transition from band 10 to band 2 ($25/2 \rightarrow 23/2$) to have a $\triangle I = 3$ character, which is also highly unlikely. Therefore, the lowest state of the cascade has been assigned a spin value of

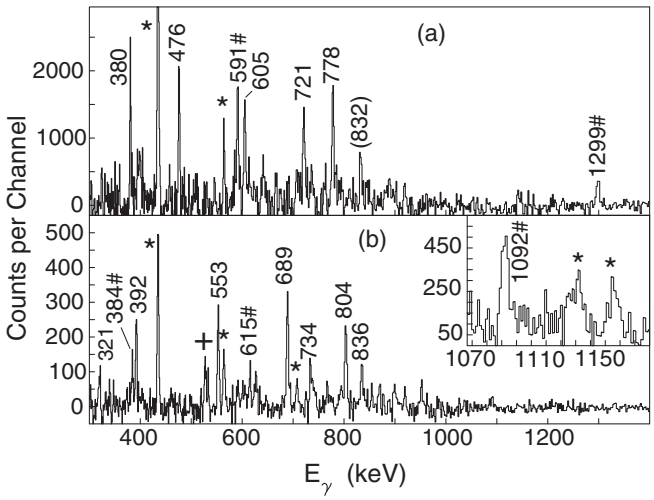

FIG. 5. (a) Triple coincidence spectrum for band 9 resulting from a sum of double gates on all band members. (b) Spectrum of band 10 resulting from a sum of triple gates set on any two band members and one of the three lowest transitions in band 1. The inset was produced by a sum of double gates on all band members. The reader is referred to the caption of Fig. 2 for the definition of the symbols.

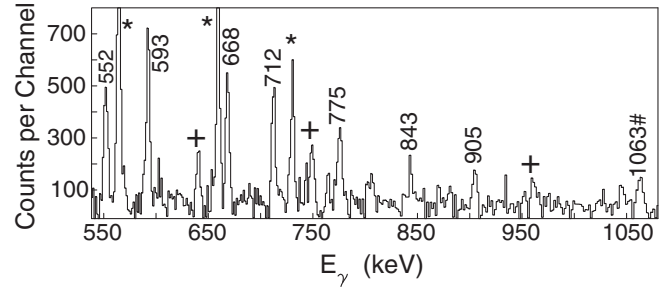

FIG. 6. Fourfold coincidence spectrum of band 11 resulting from a sum of triple gates set on any two band members and one of the five lowest transitions in band 1. The reader is referred to the caption of Fig. 2 for the definition of the symbols.

17/2. Furthermore, it was found that the rotational properties of bands 9 and 10 are remarkably similar, including their aligned angular momenta, excitation energies, and moments of inertia, and some of these properties will be discussed in Sec. IV. All these facts strongly suggest that bands 9 and 10 are signature partners and, thus have the same, positive parity. A spectrum for band 10 is shown in Fig. 5.

Band 11 is the weakest sequence in the level scheme, where the strongest γ ray of 552 keV has a relative intensity of $\sim$0.6%. Only two weak depopulating transitions could be established. A 1063-keV γ ray links the band to the positive-parity band 1, and a 974-keV transition connects it to the negative-parity band 3. The 1063-keV γ ray has a DCO ratio of 0.63(18), suggesting a probable stretched-dipole transition. Furthermore, in view of the high transition energy, an $E1$, rather than an $M1$, nature appears likely. An $M1$ transition of such high energy would be expected to exhibit an $E2$ admixture, resulting in a larger DCO ratio. Therefore, the band has been assigned a negative parity tentatively, since no further confirmation could be found. A spectrum of band 11 is displayed in Fig. 6.

IV. DISCUSSION

Cranking calculations for ^{163}Hf have been performed with the ULTIMATE CRANKER (UC) code [19–21]. The Routhian diagrams in Fig. 7 display proton and neutron orbital energies for the deformation of $\epsilon_2 = 0.20$, $\epsilon_4 = 0.02$, and $\gamma = 0^\circ$. The labeling of the quasiparticles and related orbitals closest to the Fermi surface is listed in Table II. Uppercase letters represent quasineutrons and lowercase ones quasiprotons. Each letter corresponds to a state described by a given combination of asymptotic Nilsson orbitals and by appropriate signature (α) and parity quantum numbers. Corresponding shell-model states are also given in the table.

The configurations of the bands in ^{163}Hf are assigned below, based on (i) intrinsic properties of the bands, such as the observed alignments, crossings expected at specific frequencies, excitation energies, and on (ii) systematic comparisons of these properties with those observed in neighboring nuclei. The proposed band configurations, as well as the experimentally observed band crossings are summarized in Table III. In Fig. 8, the experimental alignments of all the bands are displayed as

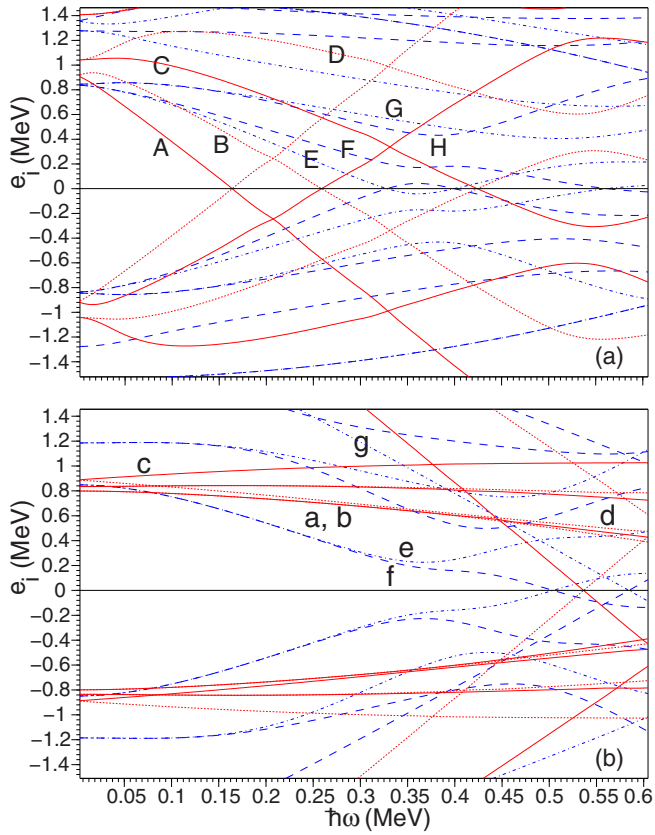

FIG. 7. (Color online) Quasiparticle diagrams for (a) neutrons and (b) protons in ^{163}Hf calculated at $\epsilon_2 = 0.20$, $\epsilon_4 = 0.02$, and $\gamma = 0^\circ$. The levels are labeled by parity and signature as $(+, +1/2)$ solid lines, $(+, -1/2)$ dotted lines, $(-, +1/2)$ dot-dashed lines, and $(-, -1/2)$ dashed lines.

a function of rotational frequency. Harris parameters $J_0 = 12\hbar^2/\text{MeV}$ and $J_1 = 80\hbar^4/\text{MeV}^3$ were chosen to subtract the angular momentum contribution of the core such that the ground-state band in ^{162}Hf [22,23] has zero initial alignment. Figure 9 provides the excitation energies of all bands in ^{163}Hf

TABLE II. Labels and alignments (i_x) of theoretical Routhians for neutrons and protons in ^{163}Hf. The spherical shell-model states represent only the main components of the wave functions, if the orbitals are mixed.

Spherical shell-model state	Nilsson orbital	$\alpha = +1/2$ Label	$\alpha = +1/2$ i_x	$\alpha = -1/2$ Label	$\alpha = -1/2$ i_x
$\nu i_{13/2}$	$\nu[651]\frac{3}{2}^+$	A	5.8	B	4.4
$\nu i_{13/2}$	$\nu[660]\frac{1}{2}^+$	C	3.0	D	1.7
$\nu h_{9/2}$	$\nu[523]\frac{5}{2}^-$	E	3.1	F	2.2
$\nu f_{7/2}$	$\nu[521]\frac{3}{2}^-$	G	1.8	H	1.9
$\pi d_{5/2}$	$\pi[402]\frac{5}{2}^+$	a	0.3	b	0.3
$\pi d_{3/2}$	$\pi[411]\frac{1}{2}^+$	c	0	d	0.3
$\pi h_{11/2}$	$\pi[514]\frac{9}{2}^-$	e	2.1	f	2.1
$\pi h_{9/2}$	$\pi[541]\frac{1}{2}^-$	g	4.1		

TABLE III. A summary of the quasiparticle configurations proposed, and the band crossing frequencies, $\hbar\omega_c$, observed in ^{163}Hf.

Band	Configurations	$\hbar\omega_c$(MeV)
1	$A \rightarrow$ABC	0.36
	ABC$\rightarrow$ABCfg	0.45
2	B	
3	$E \rightarrow$EAB	0.24
	EAB$\rightarrow$EABfg	0.43
4	FAB$\rightarrow$FABfg	0.43
5	GAB	
6	HAB	
7	$\gamma \rightarrow \gamma \otimes$ BC	0.36
8	γ	
9	AEG	
10	AEH$\rightarrow$AEHBC	0.37
11	ABCfb	

relative to a rigid-rotor reference $AI(I+1)$, where the inertia parameter A was chosen to be 7.8 keV.

A. Bands 1 and 2

Band 1 is the yrast sequence at spins below 33/2 (see Fig. 9). The band was previously identified as being built on the neutron $i_{13/2}$ orbital [14], with a configuration label A in Table II. This orbital has a large initial alignment of $\sim 6.2\hbar$, as shown in Fig. 8. The first neutron crossing (AB crossing), predicted to occur at $\hbar\omega \sim 0.22$ MeV, is blocked. Instead, the band experiences the second neutron crossing (BC crossing) at $\hbar\omega \sim 0.36$ MeV with a gain of $\sim 9\hbar$, as compared to the calculated values of 0.33 MeV and $7\hbar$ respectively. Band 1 experiences a sharp crossing at a frequency $\hbar\omega \sim 0.45$ MeV accompanied by a large alignment gain of $6.2\hbar$. The neutron CD crossing is blocked in this band. The EF crossing has been observed in several neighboring Hf isotopes, mostly with even N, where it exhibits a gradual increase of alignment of less than $2\hbar$ [22]. Thus, the sharp crossing in band 1 must involve quasiprotons rather than quasineutrons.

The onset of a proton crossing at high spins has been identified in a number of nuclides in the mass region, but only in a few of these could the bands be followed to spins high enough to delineate full alignments. One of the better studied cases is in the erbium isotopes, where the proton crossing frequency has been found to increase with neutron number. The delay was interpreted as being caused by the larger quadrupole deformation associated with the heavier isotopes [24]. A similar trend has also been investigated in the tungsten isotopes [25]. In the past decade, several Hf isotopes were investigated to very high spins so that the full proton alignment could be traced. The measured proton crossing frequencies and the magnitude of the aligned angular momenta for the lowest positive- and negative-parity bands in the Hf isotopes are summarized in Table IV. In an earlier study [26], Neffgen *et al.* suggested that these crossing frequencies should also increase with increasing neutron number, as the heavier Hf isotopes in this mass region are characterized by larger quadrupole

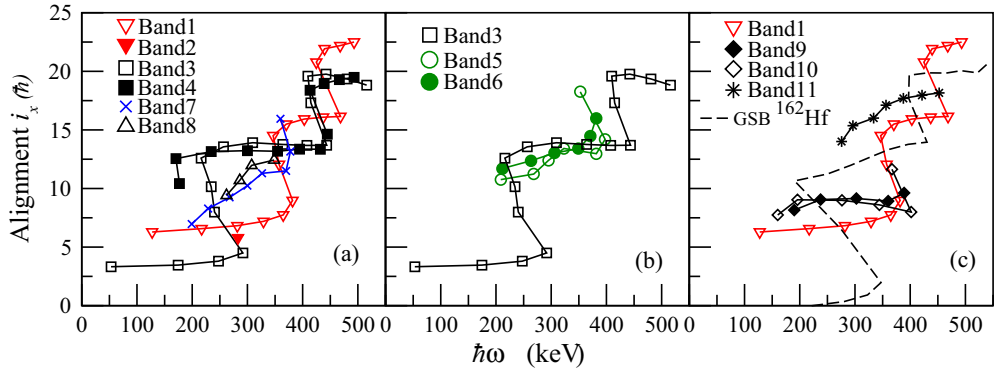

FIG. 8. (Color online) Aligned angular momentum vs rotational frequency for the bands in ^{163}Hf. Harris parameters $J_0 = 12\hbar^2$ MeV^{-1} and $J_1 = 80\hbar^4$ MeV^{-3} were used to subtract the angular momentum of the rotating core.

deformation [27,28]. The data in Table IV, spanning a chain of eleven Hf isotopes, provide solid evidence for such an effect.

The calculated lowest proton crossing is ef involving two $h_{11/2}$ protons: it is expected to generate a small alignment gain ($3 - 4.5\hbar$ for the isotopes listed), and to be gradual because of the strong interaction at the crossing. This is in contrast to the observed sharp upbend and the large alignment gain ($\sim 6\hbar$). As a result, it is suggested that the highly alignable low-Ω components of the $h_{9/2}$ orbital are involved, and the crossing is thus of "mixed" character (fg crossing) involving both the $h_{11/2}$ and the $h_{9/2}$ orbitals [18,23,33,34].

Band 2 consists of only two levels. Its excitation energy lies between those of bands 1 and 3 (see Fig. 9), suggesting that it is built on the B orbital. Indeed, its alignment of $\sim 5.5\hbar$ is also between those of bands 1 and 3 [see Fig. 8(a)], in agreement with the calculations. Both AB and BC crossings are expected to be blocked in band 2. This, however, cannot be verified in the data, since only two levels are observed. The large energy splitting between the two signatures A and B results in little population of band 2 at high spin. The observation of the $23/2^+$ and $19/2^+$ levels is due mainly to the direct feeding of theses states from levels in band 3.

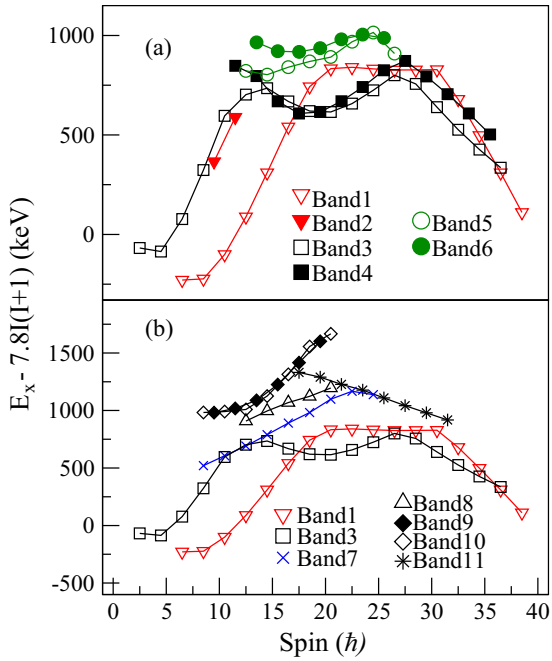

FIG. 9. (Color online) Excitation energies, minus a rigid rotor reference, as a function of spin for the bands in ^{163}Hf.

B. Bands 3 and 4

Bands 3 and 4 can be identified as signature partners from their similar rotational properties, as exhibited in Figs. 8 (alignments) and 9 (excitation energies). They are the lowest negative-parity bands, associated with neutron orbitals E and F. Band 3 undergoes the AB crossing at $\hbar\omega \sim 0.25$ MeV, with an alignment gain of $\sim 9.8\hbar$, and becomes the three-quasiparticle configuration EAB. The band has an initial alignment of $\sim 3.2\hbar$, consistent with the calculated value for orbital E. Band 4 is assigned the configuration FAB. It decays to the yrast structure near the $F \rightarrow$ FAB crossing rather than to the F band members below the backbend. It is possible that the rather large energy (1128 keV) available for the $23/2^- \rightarrow 21/2^+$ decay favors this transition over the lower-energy $23/2^- \rightarrow 19/2^-$

TABLE IV. Experimentally observed proton crossing frequencies $\hbar\omega$ (in MeV) and aligned angular momenta i_x (in $\hbar$) for the lowest positive- and negative-parity bands in Hf isotopes. The ^{163}Hf data are from the present study. The calculated equilibrium deformations, β_2, for even-A nuclei [28] are listed for reference; some experimentally measured values can be found in Refs. [29–32].

Nuclei and references	β_2	$\pi = +$		$\pi = -$	
		$\hbar\omega$	i_x	$\hbar\omega$	i_x
^{162}Hf [23]	0.170	0.41	6.0		
^{163}Hf		0.45	6.2	0.43	6.2
^{164}Hf [13]	0.195	0.49	>5.9	0.51	>7.8
^{165}Hf [26]		>0.48	–		
^{166}Hf [34]	0.221	0.51	5.6	0.48	5.4
^{167}Hf [35]		>0.50	–	>0.52	–
^{168}Hf [18]	0.246	0.55	6.1	0.54	5.2
^{169}Hf [33]		0.58	>5.8	0.56	>5.0
^{170}Hf [36]	0.260	>0.58	–	>0.58	–
^{171}Hf [37]		>0.55	>3.2	>0.58	>4.7
^{172}Hf [32]	0.271	>0.60	–		

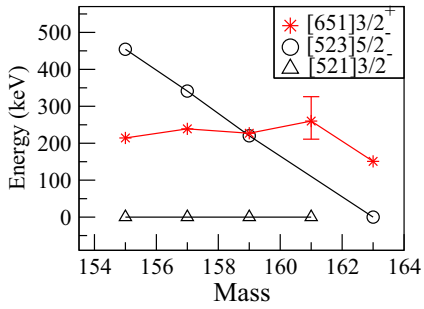

FIG. 10. (Color online) Systematics of the bandhead energies for the $\nu[523]5/2^-$ and $\nu[521]3/2^-$ bands, as well as the energies of the $13/2^+$ states in the $\nu[651]3/2^+$ bands for the $N = 91$ isotones $^{155}_{64}$Gd, $^{157}_{66}$Dy, $^{159}_{68}$Er, $^{161}_{70}$Yb, and $^{163}_{72}$Hf. See text for more discussion.

line at the band crossing. It is worth noting that a similar situation is seen in the isotone ^{161}Yb [38].

Bands 3 and 4 experience a sharp crossing at a rotational frequency $\hbar\omega \sim 0.43$ MeV with a gain of $\sim 6.2\hbar$ [see Fig. 8(a)]. The sharpness of the crossing and the alignment gain are very similar to those seen in band 1. The possibility of a neutron crossing can be ruled out since the BC, EF, and AD crossings are all blocked in bands 3 and 4, and the CD crossing is calculated to occur at rotational frequencies as high as $\hbar\omega \sim 0.55$ MeV. Thus, the crossing has been identified as the proton fg crossing. The UC calculated deformations are $\varepsilon_2 = 0.18$ for bands 3 and 4, smaller than the $\varepsilon_2 = 0.195$ for band 1. This may account for the slightly lower crossing frequencies observed in bands 3 and 4 when compared to band 1.

At the lowest spins, band 3 is associated with the $\nu[523]5/2^-$ configuration. The $5/2^-$ state is the lowest one observed not only in the band, but also in the entire level scheme. This level is likely the bandhead of band 3, and the ground state of the nucleus as well. The $13/2^+$ bandhead of band 1, the strongest band, is thus located 150.9 keV above the ground state. Figure 10 presents the systematics of bandhead energies, as well as the excitation energies of the $[651]3/2^+$ band, for the neighboring $N = 91$ isotones ^{155}Gd, ^{157}Dy, ^{159}Er, ^{161}Yb, and ^{163}Hf [39]. The ground states of the first four of these are all associated with the $[521]3/2^-$ configuration. However, the $[523]5/2^-$ orbital approaches the Fermi surface with increasing proton number and becomes the ground state in ^{163}Hf.

C. Bands 5 and 6

Figure 8(b) indicates that bands 5 and 6 have similar alignments, $1 - 2\hbar$ lower than those of bands 3 and 4. Their excitation energies are also similar to each other in most of the observed spin region, except for the lower-spin states where they interact with bands 3 and 4 [see Fig. 9(a)]. Bands 5 and 6 lie 200–300 keV higher than bands 3 and 4. They are likely signature partners associated with the configurations GAB and HAB, respectively, which are the next, higher-lying, negative-parity configurations above EAB and FAB.

The onset of another crossing is evident in bands 5 and 6 at $\hbar\omega \sim 0.38$ MeV, a value lower than the proton crossing frequency of ~ 0.43 MeV in bands 3 and 4, but higher than the BC crossing frequency of ~ 0.36 MeV in band 1. With the suggested configurations of GAB and HAB for bands 5 and 6, the BC and AD crossings are blocked. The EF crossing is calculated to occur around $\hbar\omega \sim 0.35$ MeV, with a strong interaction. Thus, the upbend in the observed alignment curves may be caused by the EF crossing, or by the EF crossing coupled with a proton crossing. In the $N = 91$ isotone, ^{159}Er, the band GAB behaves similarly, and the alignment gain at $\hbar\omega \sim 0.45$ MeV was attributed to the EF crossing coupled with proton ef crossing [40]. The same may well occur here in bands 5 and 6, but a definitive assessment cannot be made until the complete alignment is delineated.

Bands 3 and 5 are mixed at lower spins with several linking transitions between them. Interestingly, cross-talking transitions are also seen at the highest spin of band 5. A similar situation is present between bands 4 and 6 as well. This can be understood by further considering the wave functions of the bands. The $\nu[523]5/2^-$ orbital (associated with E and F) originates mainly from the $\nu h_{9/2}$ shell-model state; the $\nu[521]3/2^-$ orbital (associated with G and H) is mainly of $\nu f_{7/2}$ parentage, but contains a significant component of the $\nu h_{9/2}$ orbital. Such wave functions with several main contributions result in the actual mixing of the bands. Two sidefeeding levels, $55/2^-$ and $(59/2^-)$, feed into the $51/2^-$ level in band 4 through the 963- and 977-keV γ rays. The $55/2^-$ states in the two sequences are close in energy, which should cause mixing of them. Furthermore, the $55/2^-$ state in band 4 has a branching to the $51/2^-$ state in band 6. It is, thus, possible that the two "sidefeeding levels" are actually the continuation of band 6, where the $55/2^-$ level preferentially decays to the $51/2^-$ level in band 4 due to the strong mixing of the two sequences. Similarly, the two sidefeeding levels populating the $53/2^-$ state in band 3 could be the high-spin extension of band 5; here the mixing is more likely between the $53/2^-$ states in the two sequences.

D. Bands 7 and 8

Band 7 is closely connected to band 1 by a number of $E2$ transitions. Similar to band 1, band 7 undergoes the BC alignment [see Fig. 8(a)], suggesting that it may be associated with the A orbital. Band 7 has the same parity and signature as band 1, but is located at a higher excitation energy [see Fig. 9(b)]. A possible interpretation for band 7 is a γ-vibrational excitation coupled to band 1.

Both β- and γ-vibrational bands have been observed in the even-even $^{166-174}$Hf nuclei at low spins and they are connected to their respective ground-state bands, as summarized in Ref. [41]. These are quadrupole vibrations with $K = 0$ and $K = 2$, respectively, where K is the principal quantum number associated with the projection of the total angular momentum on the symmetry axis of the nucleus. The γ-vibrational coupling has also been reported at higher spins, e.g., in ^{169}Hf [33], ^{171}Hf [37], and ^{163}Er [42], and is known to enhance the strength of the $E2$ transitions linking the sequence to the band on which the γ vibration is built. The decay out is linked to a γ-vibrational component of the wave function, achieved by a $K = 2$ coupling in the band's configuration. For band 7 here, the $29/2^+$ level was taken as an example to estimate the $B(E2)$ values for the decay-out transitions. A transition

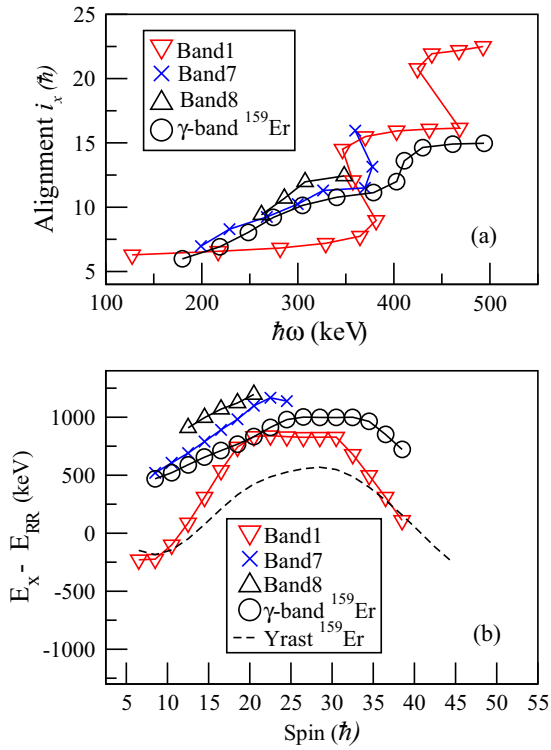

FIG. 11. (Color online) Comparison of (a) alignments and (b) excitation energies, minus a rigid-rotor reference, between γ bands in ^{163}Hf and ^{159}Er. Harris parameters $J_0 = 12\hbar^2$ MeV^{-1} and $J_1 = 80\hbar^4$ MeV^{-3} were used to subtract the angular momentum of the rotating core in ^{163}Hf. For ^{159}Er, Harris parameters were adopted from Ref. [40]. The rigid-rotor reference energies were calculated from $E_{RR} = AI(I+1)$, where the inertia parameters $A = 7.8$ and 7.7 were used for ^{163}Hf and ^{159}Er, respectively.

quadrupole moment of 5 eb is assumed for the band, based on the UC calculated deformation $\varepsilon_2 = 0.195$ for band 1. The branching ratio between the 1138-keV decay-out $E2$ γ ray and the 536-keV in-band transition is about 60%, corresponding to a $B(E2)$ value of 0.12 e^2b^2 for the decay-out transition; i.e., corresponding to 23 W.u. This value is substantially higher than expected for $E2$ decays, and is in the range of values expected for vibrational transitions. In Fig. 11, the alignment and excitation energy of band 7 are compared to those of the corresponding γ band in the $N = 91$ isotone ^{159}Er [40]. The alignments of the two bands almost overlap with each other for $\hbar\omega < 0.36$ MeV, but the BC crossing is delayed in ^{159}Er. There is a gradual gain of $\sim 3\hbar$ in alignment for the two bands between the frequencies of 0.2 and 0.35 MeV. The nature of this upturn is unclear. The vibrational excitation energy between the $17/2^+$ state in band 7 and the $13/2^+$ level in band 1 is 999 keV. The value is higher than the corresponding energy of 864 keV in ^{159}Er [40], and is also substantially higher than the energy of 810 keV for the $2^+ \rightarrow 0^+$ γ ray from the γ band to the ground state sequence in ^{166}Hf [43]. For the heavier even-even Hf isotopes, $^{168-174}$Hf, the vibrational energy increases systematically with mass number [18,41].

Band 8 is very similar to band 7. Both of them have positive parity, positive signature, and are characterized by strong $E2$ branchings to band 1. Their alignment patterns are similar with close values, as can be seen in Fig. 11. Band 8 has higher excitation energy than band 7. In an odd nucleus, the γ vibration ($K = 2$) can couple to a band with a given K value in two opposite directions. Band 1 in ^{163}Hf is associated with $i_{13/2}$ neutron with a K value close to 3/2, which can lead to two γ-vibrational bands with K values of 7/2 and 1/2. Therefore, band 8 is proposed to be the second γ-vibrational band built on band 1.

E. Bands 9 and 10

Bands 9 and 10 have identical rotational properties, such as their alignments [Fig. 8(c)], excitation energies [Fig. 9(b)], and moments of inertia (not shown here). Consequently, they are identified as signature partners. Their alignments are $\sim 2.5\hbar$ higher than that of band 1, suggesting that they are associated with three-quasiparticele configurations, even at the lowest spins. The sharp upbend of band 10 at high spin is associated with the BC crossing, indicating that its configuration involves orbital A. Among all possible three-quasiparticle configurations, including three-quasineutron or one-quasineutron-plus-two-quasiproton configurations, the most probable ones for the bands are likely the three-neutron configurations AEG (for band 9) and AEH (for band 10), which are the next higher configurations above the GAB/HAB ones associated with bands 5 and 6. The difference between configurations AEG and GAB is that the former contains orbital E, while the latter contains the B orbital. Orbital E has a higher excitation energy and a smaller alignment than orbital B, and the splitting between these two increases at higher rotational frequency (see Fig. 7). This accounts for the differences in excitation energy and alignments between bands 9 and 5 (see Figs. 8 and 9). A similar reason leads to the differences between bands 10 (associated with configuration AEH) and 6 (associated with HAB). The proposed configurations have positive parity, in agreement with the experimental data.

F. Band 11

The trajectory of band 11 in the excitation energy plot of Fig. 9(b) is essentially straight. This points to this sequence having an intrinsic configuration distinctive from all others and, thus, it would not be expected to interact with other bands. The deexcitation occurs within the band, and decay-out transitions are observed only for the lowest two levels, feeding bands 1 and 3. The band starts at $\hbar\omega \sim 0.27$ MeV with $\sim 14\hbar$ initial alignment [see Fig. 8(c)], and its alignment curve is parallel to, but $\sim 2\hbar$ higher than, that of band 1 over most of the observed spin range. This indicates that the band may have a five-quasiparticle configuration, i.e., the configuration ABC plus two additional quasiparticles.

A five-neutron ABCEF configuration is unlikely, since, as mentioned previously, the EF crossing is not expected below $\hbar\omega \sim 0.35$ MeV. In addition, the sequence has a proposed negative parity, which does not match the positive parity of the ABCEF configuration. Furthermore, no sign of an upbend is present at the highest frequency of $\hbar\omega \sim 0.45$ MeV, where proton alignments occur in other bands traced to such high frequencies. This fact points to another scenario where this

five-quasiparticle configuration may involve protons already at lower frequencies. That is, unlike the high-spin proton crossings at $\hbar\omega \sim 0.45$ MeV observed in other bands, the proton excitations at lower frequency, but higher excitation energy, must be considered.

The most likely configuration for band 11 is ABCfb, which involves the excitations of proton $[514]9/2^-$ and $[402]5/2^+$ states. Such a configuration has a negative parity and, according to UC calculations, generates $\sim 2.5\hbar$ more alignment than the ABC configuration, in agreement with the observed alignments in Fig. 8(c). The calculated band is $\sim$1 MeV higher than band 1 at $\hbar\omega \sim 0.3$ MeV [see Fig. 7(b)], which is higher than the observed $\sim$0.7-MeV value [see Fig. 9(b)]. The proton orbitals a and b are degenerate, the orbitals e and f split apart at higher rotational frequencies, and the orbital f has lower energy. Thus, the configuration ABCfb is considered more likely than ABCea as an assignment for band 11. With the present interpretation, a signature degenerate partner to band 11, ABCfa, should also be populated. But for such a weak band, it is probably not unexpected that only one signature is observed.

G. Search for TSD band

Since bands associated with a stable triaxial shape have been identified in several close neighbors of ^{163}Hf, e.g., $^{164}_{72}$Hf [13] and $^{161-165}_{71}$Lu [3,5,7–9], as well as in the lighter even nuclei $^{160}_{70}$Yb [44] and $^{158}_{68}$Er [45], the possibility that band 11 is associated with a TSD structure has also been examined. All known TSD bands in this mass region are based on quasiparticle excitations, and the same holds for wobbling bands. In every instance one or more aligned quasiprotons occupying the $i_{13/2}$ intruder orbital are involved in the TSD configuration. A single $i_{13/2}$ quasiproton would generate $\sim 6\hbar$ of aligned angular momentum. Furthermore, these TSD bands are also characterized by dynamical moments of inertia substantially larger than those of the normal deformed bands. Neither of these characteristics is consistent with the properties of band 11 or of the other sequences discussed above.

The issue of whether a TSD minimum can possibly exist in ^{163}Hf should be considered in view of the present failure to observe any relevant signal. In this context, it is worthwhile to recall that, while the present measurement was optimized for the production of ^{164}Hf, ^{163}Hf was only a byproduct. As a result, high-spin states were delineated up to $77/2\hbar$, a value significantly lower than those of 48 and $\sim 61\hbar$ characterizing the TSD bands in ^{164}Hf [13] and ^{168}Hf [12]. Thus, a TSD sequence may well be present in ^{163}Hf at higher spins and/or higher excitation energy: only a dedicated, high-statistics measurement favoring the population of the higher-spin states of ^{163}Hf may provide the answer. On the other hand, numerous theoretical studies, based on different approaches—see, e.g., Refs. [46–53]—have investigated the properties of TSD structures in even-N nuclei, with both odd and even Z, but few of these discuss the characteristics of similar TSD sequences in odd-N nuclei. In particular, no calculation is available for ^{163}Hf. More generally, it has proved challenging to predict the properties of TSD minima in specific nuclei of the region, even those of nuclei differing by only one or two nucleons from the well-established cases. Further theoretical work is clearly needed. The present work extends the knowledge on collective motion in ^{163}Hf significantly and, in doing so, provides an improved basis for both theoretical investigations and a dedicated experiment.

V. SUMMARY

Excited states in ^{163}Hf have been investigated. Two previously known bands have been extended up to high spins of $77/2^+$ and $71/2^-$, respectively, and nine new bands have been identified. All the bands have been linked to each other. Spins and parity have been assigned based on DCO ratio measurements. Intrinsic configurations have been proposed for the bands, based on the observed band crossings, aligned angular momenta, and excitation energies, with the help of cranking calculations using the ULTIMATE CRANKER code, as well as systematic comparisons with neighboring nuclei. Bands associated with several three-quasineutron configurations have been established, together with a five-quasiparticle band including two quasiprotons. Two new sequences are proposed to correspond to γ-vibrational bands coupled to the same $i_{13/2}$ neutron band. Proton crossings at $\hbar\omega \sim 0.45$ MeV have been observed in both positive- and negative-parity bands and traced to full alignments. The new results, combined with recent data in neighboring Hf isotopes, point to a delay of the proton crossing frequency increasing with quadrupole deformation from ^{162}Hf to ^{172}Hf. A negative-parity band was suggested to be associated with the $\nu h_{9/2}$ orbital and its $5/2^-$ bandhead state is proposed to be the ground state of the ^{163}Hf nucleus. Extensive band searches were performed, but failed to reveal a TSD band similar to those reported in the island of TSD sequences centered around $A \sim 165$. Additional theoretical investigations and a better experiment dedicated to the population of high-spin states in ^{163}Hf are needed to address the issue further.

ACKNOWLEDGMENTS

The authors thank the ANL operations staff at Gammasphere and gratefully acknowledge the efforts of J. P. Greene for the target preparation. This material was based upon work supported by the US Department of Energy, Office of Science, Office of Nuclear Physics, under Award No. DE-FG02-95ER40939 (MSU) and under Contract No. DE-AC02-06CH11357 (ANL), and by the National Science Foundation under Grant No. PHY-1203100 (USNA). This research used resources of ANL's ATLAS facility, which is a DOE Office of Science User Facility.

[1] S. Ødegård *et al.*, Phys. Rev. Lett. **86**, 5866 (2001).
[2] D. R. Jensen *et al.*, Phys. Rev. Lett. **89**, 142503 (2002).
[3] G. Schönwaßer *et al.*, Phys. Lett. B **552**, 9 (2003).
[4] H. Amro *et al.*, Phys. Lett. B **553**, 197 (2003).
[5] P. Bringel *et al.*, Eur. Phys. J. A **24**, 167 (2005).
[6] D. J. Hartley *et al.*, Phys. Rev. C **80**, 041304(R) (2009).

[7] P. Bringel *et al.*, Eur. Phys. J. A **16**, 155 (2003).
[8] D. R. Jensen *et al.*, Eur. Phys. J. A **19**, 173 (2004).
[9] P. Bringel *et al.*, Phys. Rev. C **75**, 044306 (2007).
[10] N. S. Pattabiraman *et al.*, Phys. Lett. B **647**, 243 (2007).
[11] H. Amro *et al.*, Phys. Lett. B **506**, 39 (2001).
[12] R. B. Yadav *et al.*, Phys. Rev. C **78**, 044316 (2008).
[13] J. C. Marsh *et al.*, Phys. Rev. C **88**, 041306(R) (2013).
[14] K. P. Blume *et al.*, Nucl. Phys. A **464**, 445 (1987).
[15] I. Y. Lee, Nucl. Phys. A **520**, 641 (1990).
[16] D. C. Radford, Nucl. Instrum. Methods Phys. Res., Sect. A **361**, 297 (1995).
[17] K. S. Krane, R. M. Steffen, and R. M. Wheeler, Nucl. Data Tables **11**, 351 (1973).
[18] R. B. Yadav *et al.*, Phys. Rev. C **80**, 064306 (2009).
[19] R. Bengtsson (private communication).
[20] T. Bengtsson, Nucl. Phys. A **496**, 56 (1989).
[21] T. Bengtsson, Nucl. Phys. A **512**, 124 (1990).
[22] C. R. Bingham *et al.*, J. Phys. G **14**, L77 (1988).
[23] H. Hübel, M. Murzel, E. M. Beck, H. Kluge, A. Kuhnert, K. H. Maier, J. C. Bacelar, M. A. Deleplanque, R. M. Diamond, and F. S. Stephens, Z. Phys. A **329**, 289 (1988).
[24] M. Riley *et al.*, Phys. Lett. B **135**, 275 (1984).
[25] K. Theine *et al.*, Nucl. Phys. A **548**, 71 (1992).
[26] M. Neffgen, E. M. Beck, H. Hübel, J. C. Bacelar, M. A. Deleplanque, R. M. Diamond, F. S. Stephens, and J. E. Draper, Z. Phys. A **344**, 235 (1992).
[27] R. Bengtsson, S. Frauendorf, and F. R. May, Atom. Data Nucl. Data Tables **35**, 15 (1986).
[28] W. Nazarewicz, M. A. Riley, and J. D. Garrett, Nucl. Phys. A **512**, 61 (1990).
[29] S. Raman, C. H. Malarkey, W. T. Milner, C. W. Nestor, and P. H. Stelson, At. Data Nucl. Data Tables **36**, 1 (1987).
[30] W. B. Gao, I. Y. Lee, C. Baktash, R. Wyss, J. H. Hamilton, C. M. Steele, C. H. Yu, N. R. Johnson, and F. K. McGowan, Phys. Rev. C **44**, 1380 (1991).
[31] D. M. Cullen *et al.*, Nucl. Phys. A **673**, 3 (2000).
[32] D. M. Cullen, A. T. Reed, D. E. Appelbe, A. N. Wilson, E. S. Paul, R. M. Clark, P. Fallon, I. Y. Lee, A. O. Macchiavelli, and R. W. MacLeod, Nucl. Phys. A **638**, 662 (1998).
[33] K. A. Schmidt *et al.*, Eur. Phys. J. A **12**, 15 (2001).
[34] D. R. Jensen *et al.*, Eur. Phys. J. A **8**, 165 (2000).
[35] M. Cromaz *et al.*, Phys. Rev. C **59**, 2406 (1999).
[36] A. Neußer-Neffgen *et al.*, Phys. Rev. C **73**, 034309 (2006).
[37] Y. C. Zhang *et al.*, Phys. Rev. C **85**, 064307 (2012).
[38] L. L. Riedinger, Nucl. Phys. A **347**, 141 (1980).
[39] R. B. Firestone *et al.*, *Table of Isotopes* (John Wiley & Sons, New York, 1996), Vol. II.
[40] M. Mustafa *et al.*, Phys. Rev. C **84**, 054320 (2011).
[41] E. A. McCutchan *et al.*, Phys. Rev. C **77**, 054304 (2008), and references therein.
[42] G. B. Hagemann *et al.*, Nucl. Phys. A **618**, 199 (1997).
[43] E. A. McCutchan, N. V. Zamfir, R. F. Casten, M. A. Caprio, H. Ai, H. Amro, C. W. Beausang, A. A. Hecht, D. A. Meyer, and J. J. Ressler, Phys. Rev. C **71**, 024309 (2005).
[44] A. Aguilar *et al.*, Phys. Rev. C **77**, 021302(R) (2008).
[45] X. Wang *et al.*, Phys. Lett. B **702**, 127 (2011).
[46] I. Hamamoto, Phys. Rev. C **65**, 044305 (2002).
[47] R. Bengtsson and H. Ryde, Eur. Phys. J. A **22**, 355 (2004).
[48] M. Matsuzaki, Y. R. Shimizu, and K. Matsuyanagi, Phys. Rev. C **69**, 034325 (2004).
[49] B. G. Carlsson, Int. J. Mod. Phys. E **16**, 634 (2007).
[50] K. Sugawara-Tanabe and K. Tanabe, Phys. Rev. C **82**, 051303(R) (2010).
[51] A. Kardan, I. Ragnarsson, H. Miri-Hakimabad, and L. Rafat-Motevali, Phys. Rev. C **86**, 014309 (2012).
[52] Y. Shi, J. Dobaczewski, S. Frauendorf, W. Nazarewicz, J. C. Pei, F. R. Xu, and N. Nikolov, Phys. Rev. Lett. **108**, 092501 (2012).
[53] S. Frauendorf and F. Dönau, Phys. Rev. C **89**, 014322 (2014).